Cu(I) complex based on 6*H*-indolo[2,3-*b*]quinoxaline: structure and electrocatalytic property for hydrogen evolution reaction from water

Pan Zhang, [a] Xin Yang, [b] Penggang Jiang, [a] Junli Yin, [a] Yun Gong [*a] and Jianhua Lin [*a, c]

[a] *Department of Applied Chemistry, College of Chemistry and Chemical Engineering, Chongqing University, Chongqing 400030, P. R. China Tel: +86-023-65106150 E-mail: gongyun7211@cqu.edu.cn*

[b] *Chongqing Foreign Language School, Chongqing 400039, P. R. China*

[c] *State Key Laboratory of Rare Earth Materials Chemistry and Applications, College of Chemistry and Molecular Engineering, Peking University, Beijing 100871, P. R. China Tel: +86-010-62753541 E-mail: jhlin@pku.edu.cn; jhlin@cqu.edu.cn*

Determination of Faradaic Efficiency

Controlled potential electrolyses were conducted in a 50 mL 0.05M phosphate buffer aqueous solution (pH = 6.8, H_3PO_4/KOH) at an applied potential of □-1.5 V vs SCE (η = -0.86 V) for 1 hour. The pH change of the solution during the electrolysis was recorded with a pH meter. Assuming 100% Faradaic efficiency, the theoretical pH change over time can be calculated by the equation of pH = 14 + lg {Σ(It)/(FV)}, where I = current (A), t = time (s), F = Faraday constant (96485 C/mol), V = solution volume (0.05 L). [1] The amount of H_2 evolved was determined using gas chromatography (GC, 7890A, thermal conductivity detector (TCD), Ar carrier, Agilent). The theoretical (assuming 100%

Faradic efficiency) hydrogen volume is based on the amount of consumed charge during the course of electrolysis.

Table S1 Selected bond lengths (Å) and angles (º) for **HL** and complex **1**

HL			
N(1)-C(1)	1.314(5)	N(1)-C(4)	1.376(5)
N(2)-C(2)	1.241(6)	N(2)-C(3)	1.427(6)
N(3)-C(1)	1.346(5)	N(3)-C(9)	1.392(5)
C(1)-N(1)-C(4)	112.3(4)	C(2)-N(2)-C(3)	112.7(5)
C(1)-N(3)-C(9)	110.5(4)	N(1)-C(1)-N(3)	127.0(4)
N(1)-C(1)-C(2)	126.1(4)	N(3)-C(1)-C(2)	106.9(4)
Complex 1			
Cu(1)-N(3)#1	1.863(4)	Cu(1)-N(1)	1.889(4)
Cu(1)-Cu(1)#1	2.6367(11)	N(1)-C(7)	1.323(6)
N(1)-C(1)	1.389(5)	N(3)-C(7)	1.338(6)
N(3)-C(9)	1.405(6)	N(2)-C(8)	1.162(7)
N(3)#1-Cu(1)-N(1)	171.95(15)	N(3)#1-Cu(1)-Cu(1)#1	85.10(11)
N(1)-Cu(1)-Cu(1)#1	86.85(11)	C(7)-N(1)-C(1)	113.3(4)
C(7)-N(3)-C(9)	108.1(4)	N(1)-C(7)-N(3)	126.3(4)
N(1)-C(7)-C(8)	127.3(4)	N(3)-C(7)-C(8)	106.4(4)

Symmetry transformations used to generate equivalent atoms:

#1 -x+2, -y-1, -z+2

Table 3 The centroid-centroid (CC) distance (Å) and perpendicular (P) distance (Å) involving π···π stacking interactions for complex **1**

Plane	Plane	CC distance	P distance
N3/C7-C9/C14	N1A-N2A/C1A-C2A/C7A-C8A	3.6564	3.3052
N3/C7-C9/C14	C1B-C6B	4.0420	3.3431
N1-N2/C1-C2/C7-C8	N1A-N2A/C1A-C2A/C7A-C8A	4.1310	3.3053
N1-N2/C1-C2/C7-C8	N1B-N2B/C1B-C2B/C7B-C8B	4.1980	3.3381
N1-N2/C1-C2/C7-C8	C1B-C6B	3.8067	3.3439

Symmetry transformations used to generate equivalent atoms: A *-x*,2-*y*,-*z* B 1-*x*,2-*y*,-*z*

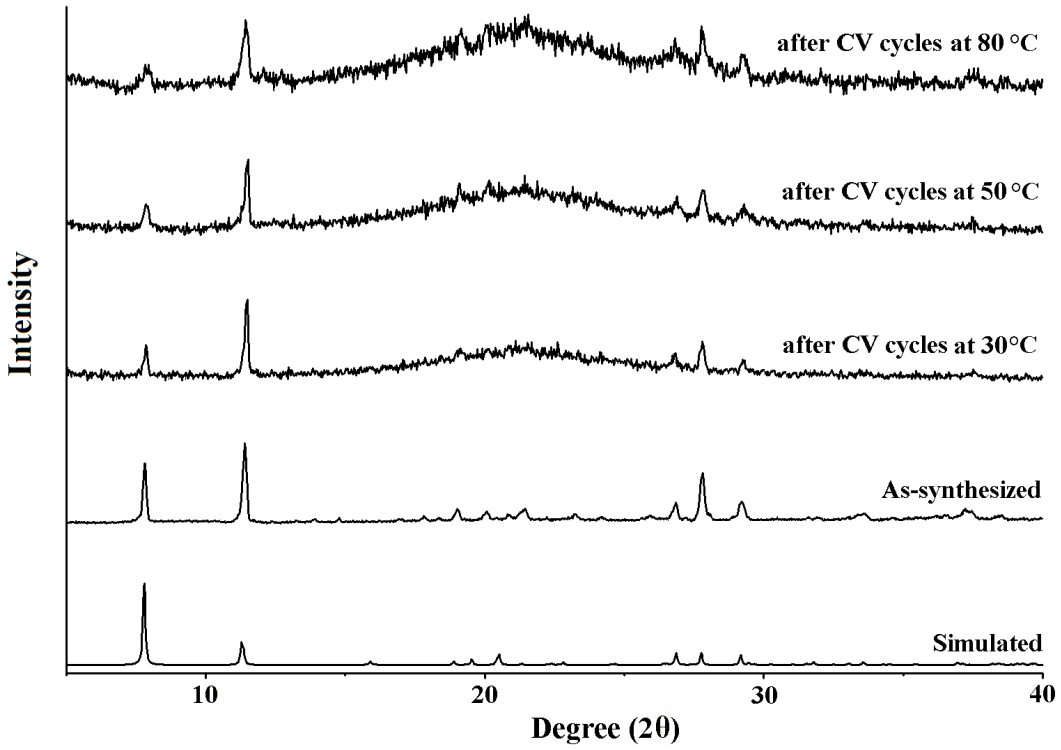

Fig. S1 The powder XRD patterns for complex **1**.

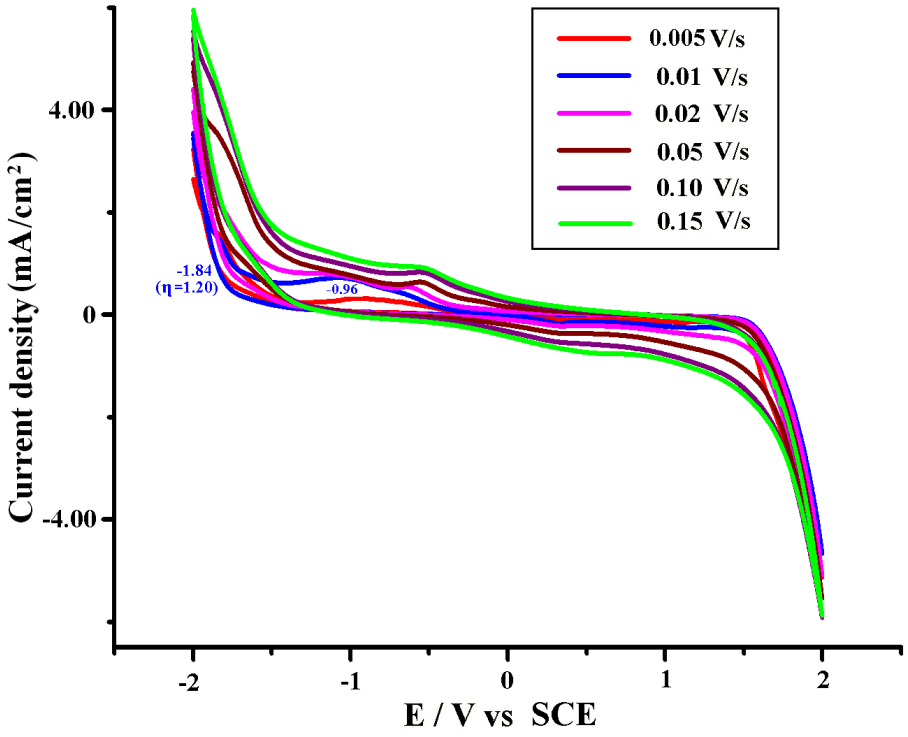

Fig. S2 CVs of the bare **GCE** in 0.05 M phosphate buffer aqueous solution (pH = 6.8, H_3PO_4/KOH, 50 mL) at 30 ℃ at different sweep rates.

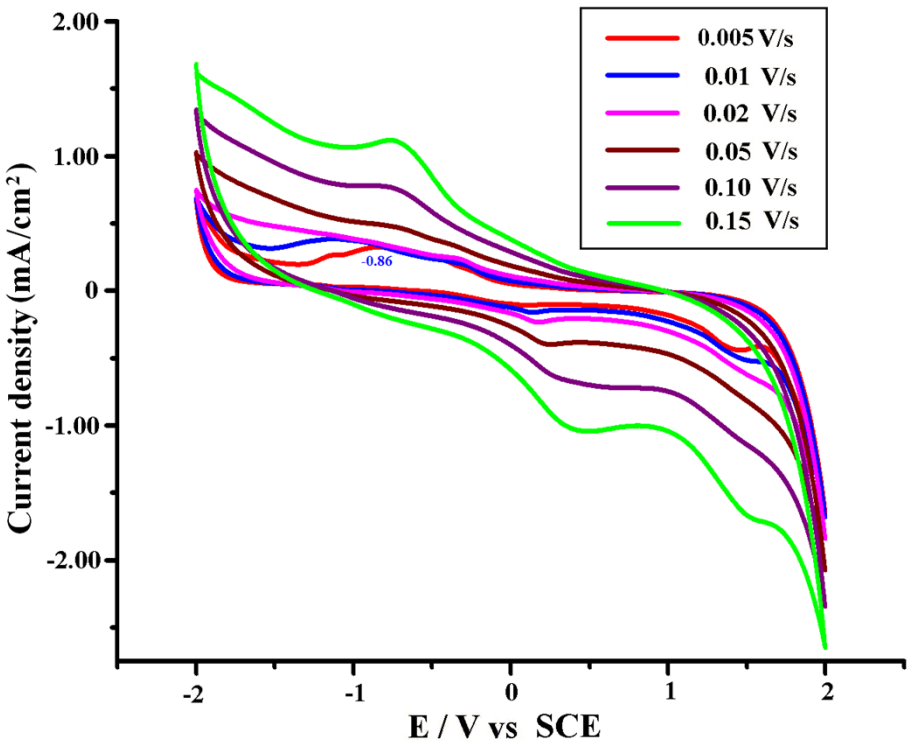

Fig. S3 CVs of **HL-GCE** in 0.05 M phosphate buffer aqueous solution (pH = 6.8, H_3PO_4/KOH, 50 mL) at 30 ℃ at different sweep rates.

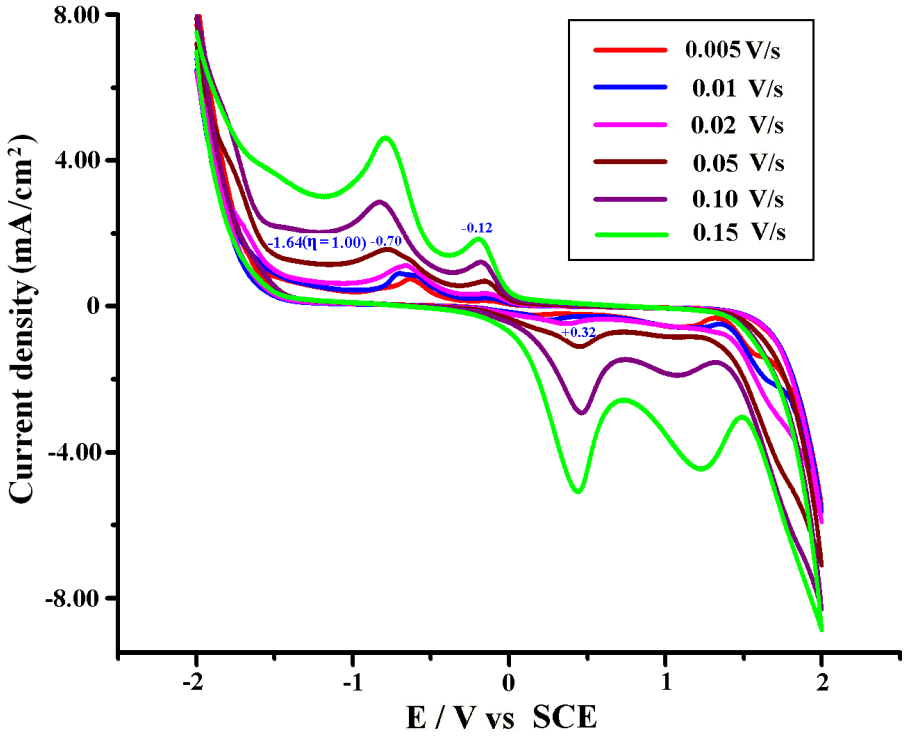

Fig. S4 CVs of **1-GCE** in 0.05 M phosphate buffer aqueous solution (pH = 6.8, H_3PO_4/KOH, 50 mL) at 30 ℃ at different sweep rates.

(a)

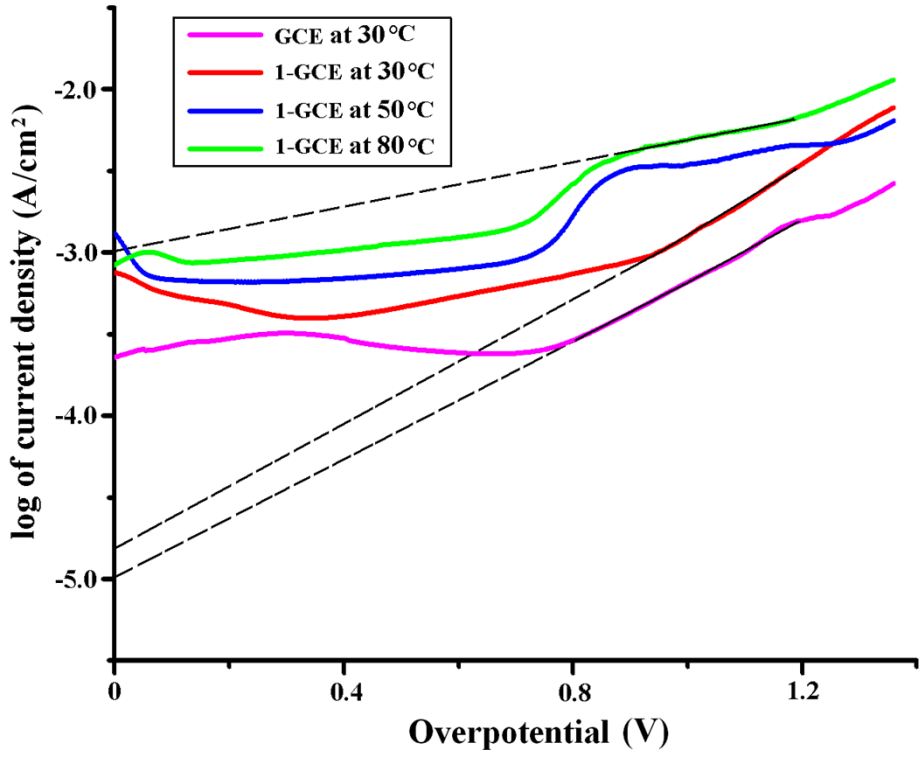
GCE at 30 °C
1-GCE at 30 °C
1-GCE at 50 °C
1-GCE at 80 °C
log of current density (A/cm²)
-2.0
-3.0
-4.0
-5.0
0
0.4
0.8
1.2
Overpotential (V)

(b)

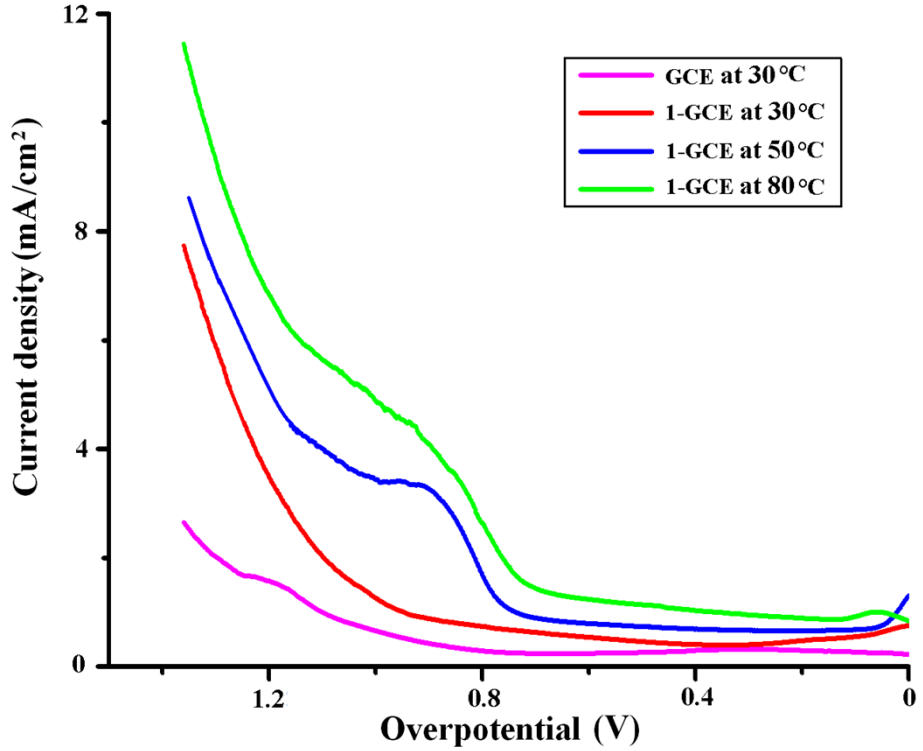
GCE at 30 °C
1-GCE at 30 °C
1-GCE at 50 °C
1-GCE at 80 °C
Current density (mA/cm²)
12
8
4
0
1.2
0.8
0.4
0
Overpotential (V)

Fig. S5 Tafel plots of *log* current intensity (*i*) against overpotential η for the HER at the bare **GCE** and **1-GCE** in 0.05 M phosphate buffer aqueous solution (pH = 6.8, H_3PO_4/KOH, 50 mL) at sweep rates of 0.01 $V \cdot s^{-1}$ under different temperatures (The linear part of the Tafel curves denoted in black dotted lines with the intercept at the *y* axis) (**a**); Current intensity (*i*) / overpotential (η) diagrams (**b**) for the HER.

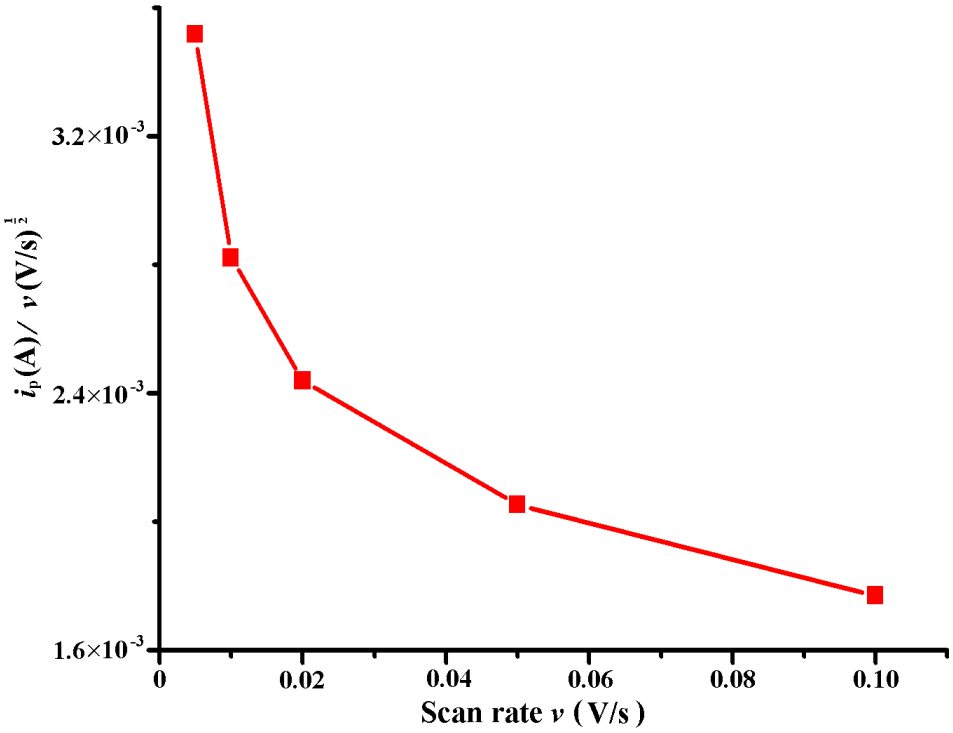

Fig. S6 The plots of i_p / $v^{1/2}$ against scan rate *v* at **1-GCE** under the room temperature of 30 °C.

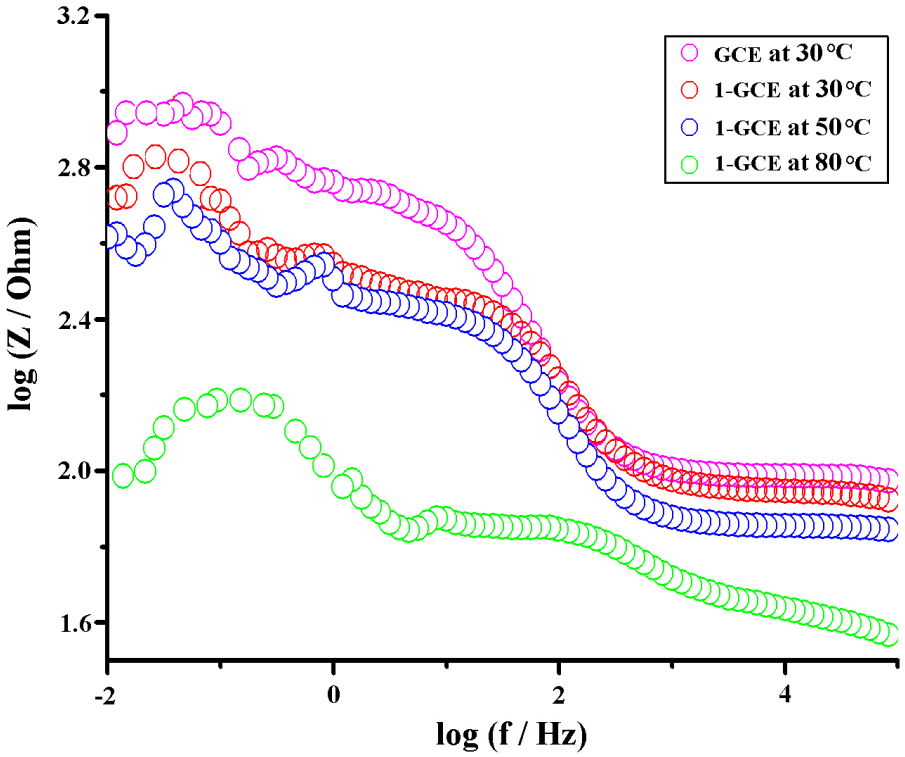

Fig. S7 Bode plots (log of impedance magnitude vs. log f) of the three-electrode systems in 0.05 M phosphate buffer aqueous solution (pH = 6.8, H_3PO_4/KOH, 50 mL) at the initial potential of -1.5 V with the bare **GCE** and **1-GCE** as working electrodes, respectively under different temperatures.

(a)

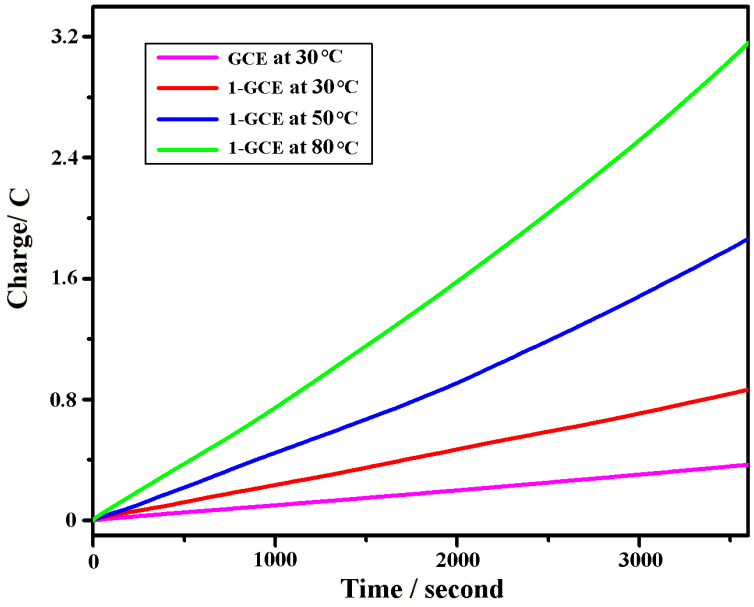

(b)

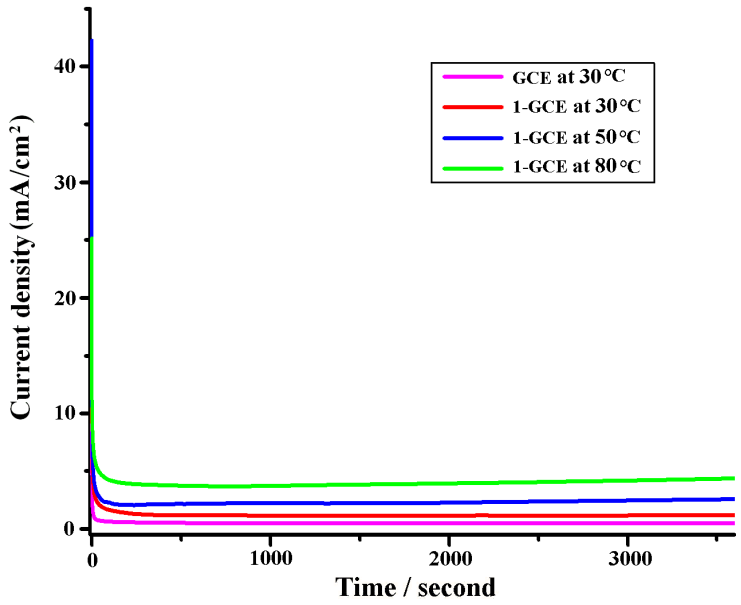

Fig. S8 Controlled potential electrolysis of the bare **GCE** and **1-GCE** in 0.05 M phosphate buffer aqueous solution (pH = 6.8, H_3PO_4/KOH, 50 mL) under different temperatures, showing charge buildup versus time (**a**) and plot of current density against time (**b**) with an applied potential of -1.5 V vs SCE (η = 0.86 V).

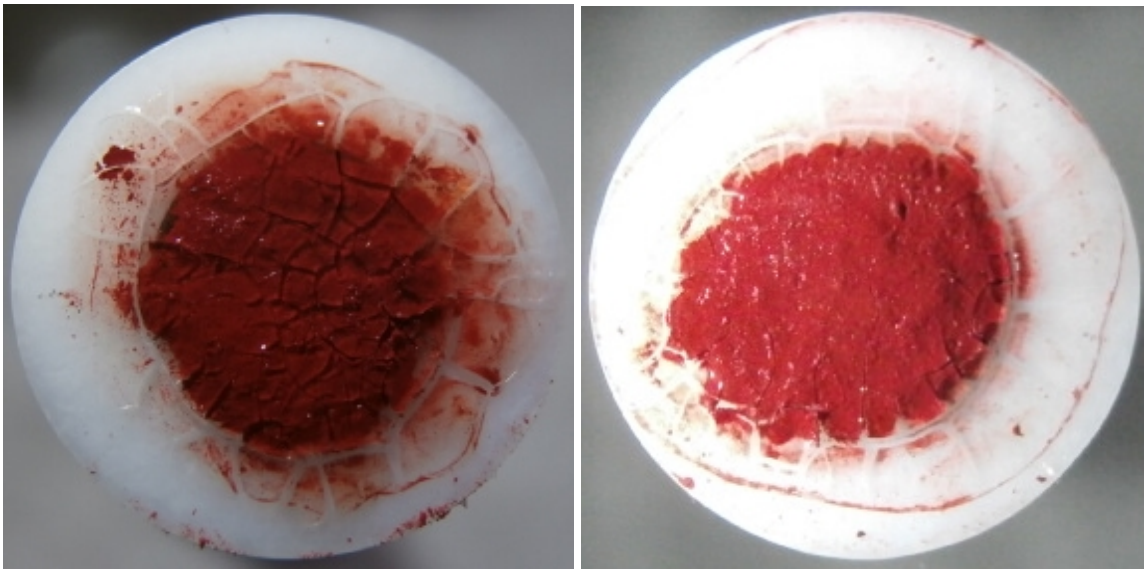

Fig. S9 The images of **1-GCE** before (left) and after (right) one hundred of CV cycles in the potential range of-2.0 ~ 2.0 V vs SCE.

(a)

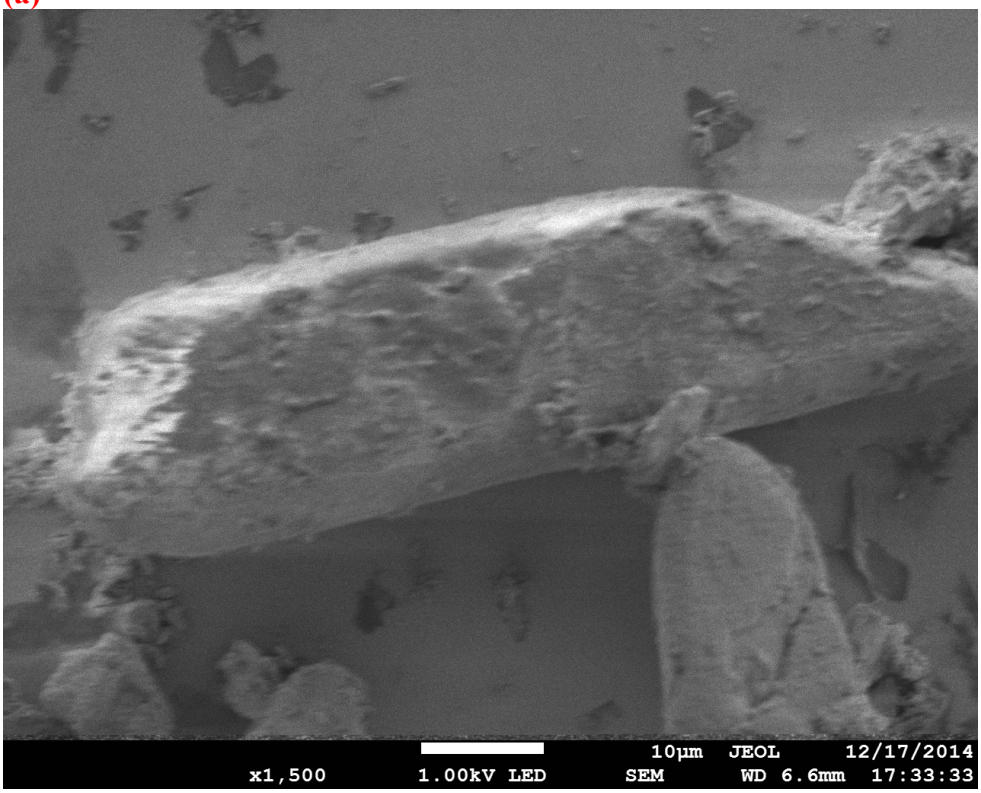
x1,500 1.00kV LED
10µm JEOL
SEM
12/17/2014
WD 6.6mm 17:33:33

(b)

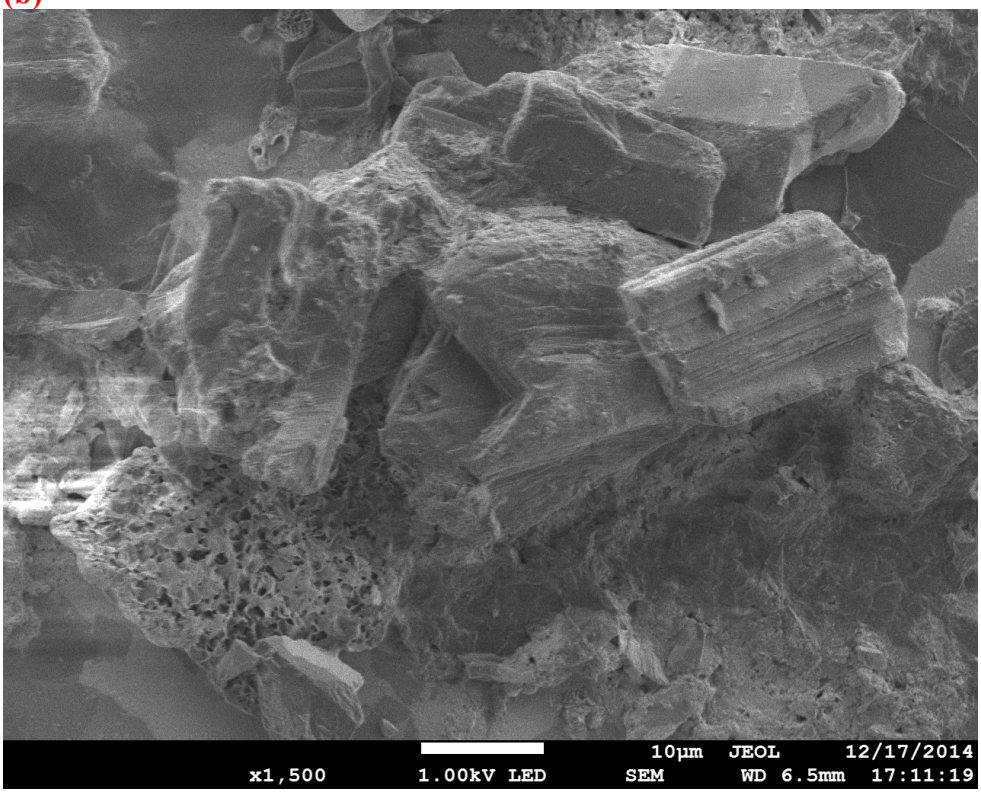
x1,500 1.00kV LED
10µm JEOL
SEM
12/17/2014
WD 6.5mm 17:11:19

(c)

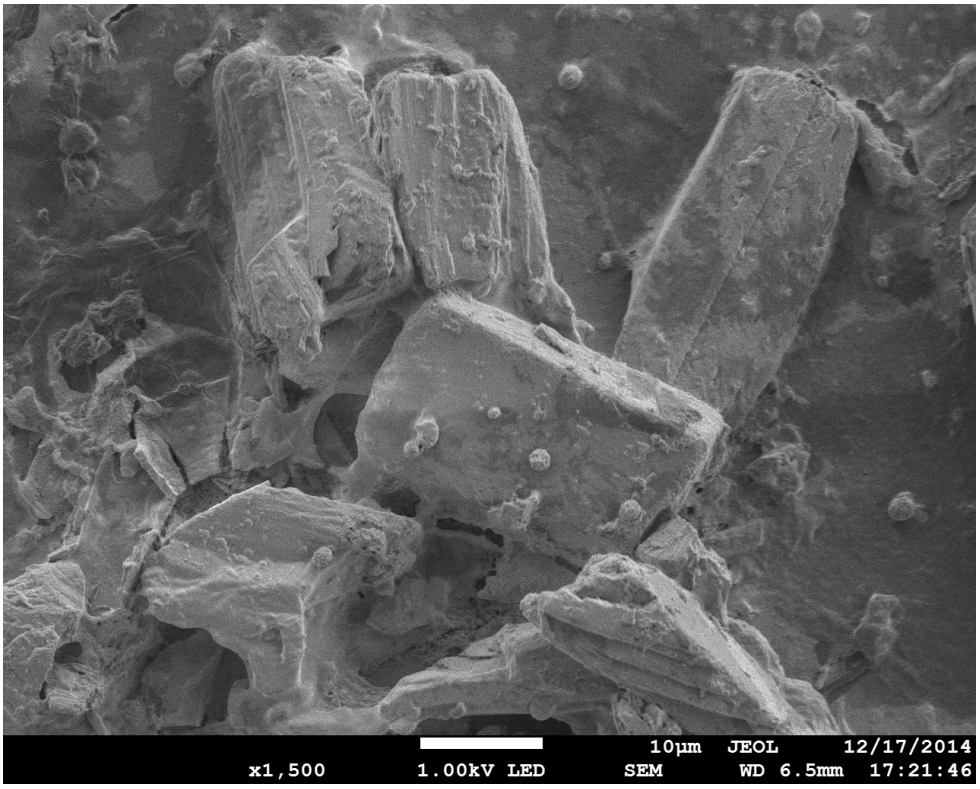

(d)

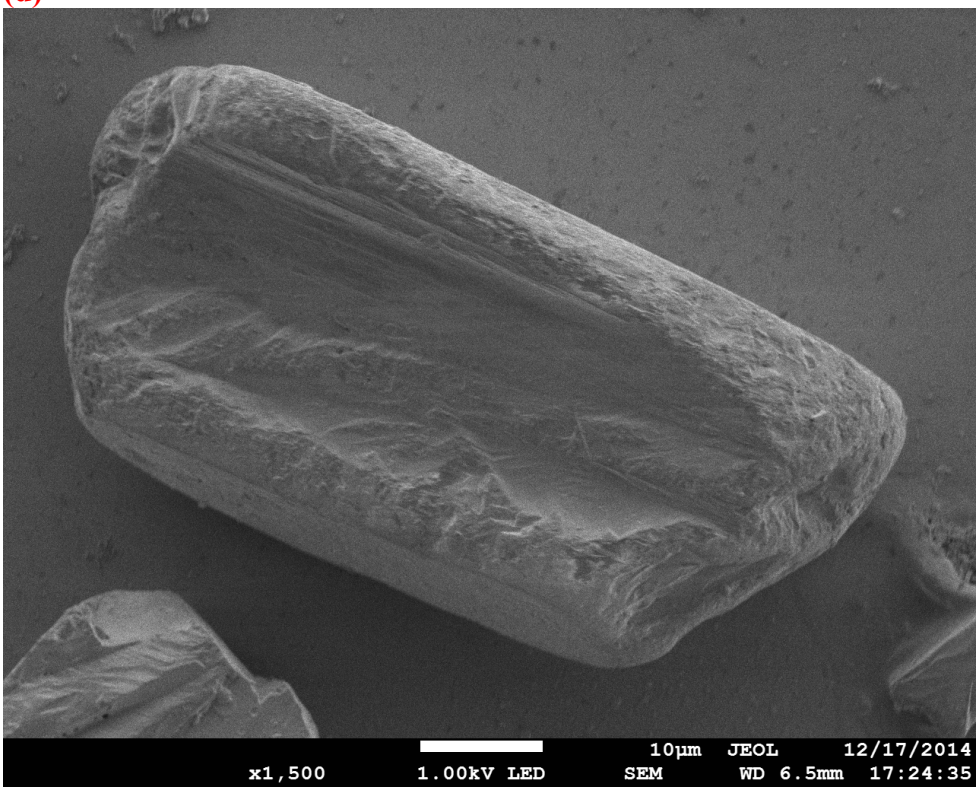

Fig. S10 The SEM images of complex **1** before (**a**) and after the electrochemical experiments at 30 °C (**b**), 50 °C (**c**) and 80 °C (**d**), respectively.

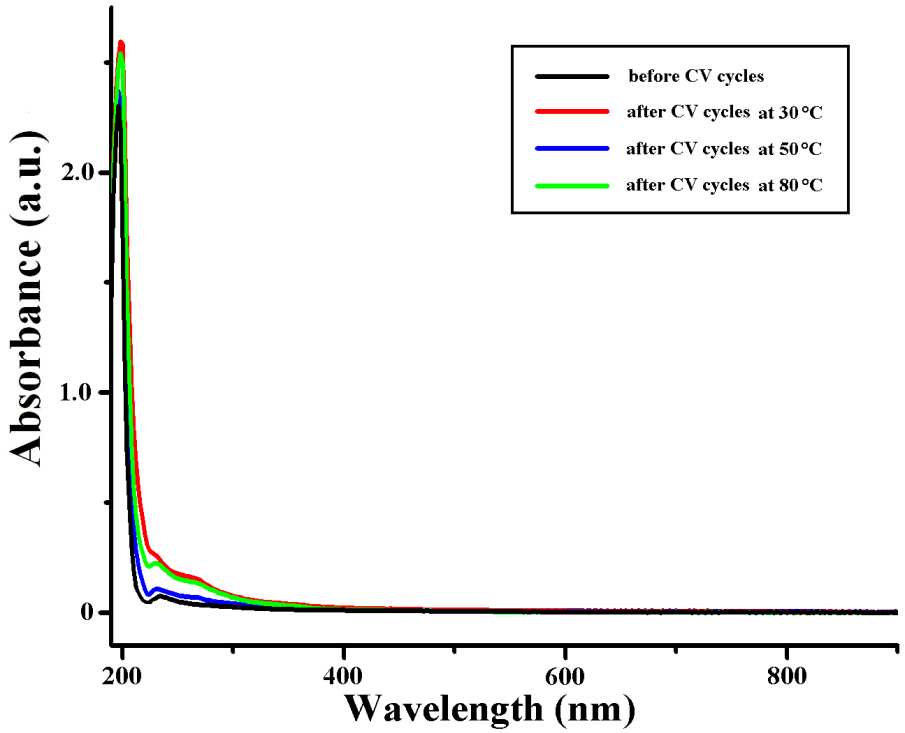

Fig. S11 UV-vis absorption spectra for the phosphate buffer aqueous solution (pH = 6.8, H_3PO_4/KOH) in the presence of **1-GCE** before and after one hundred of CV cycles in the potential range of-2.0 ~ 2.0 V vs SCE at different temperatures.

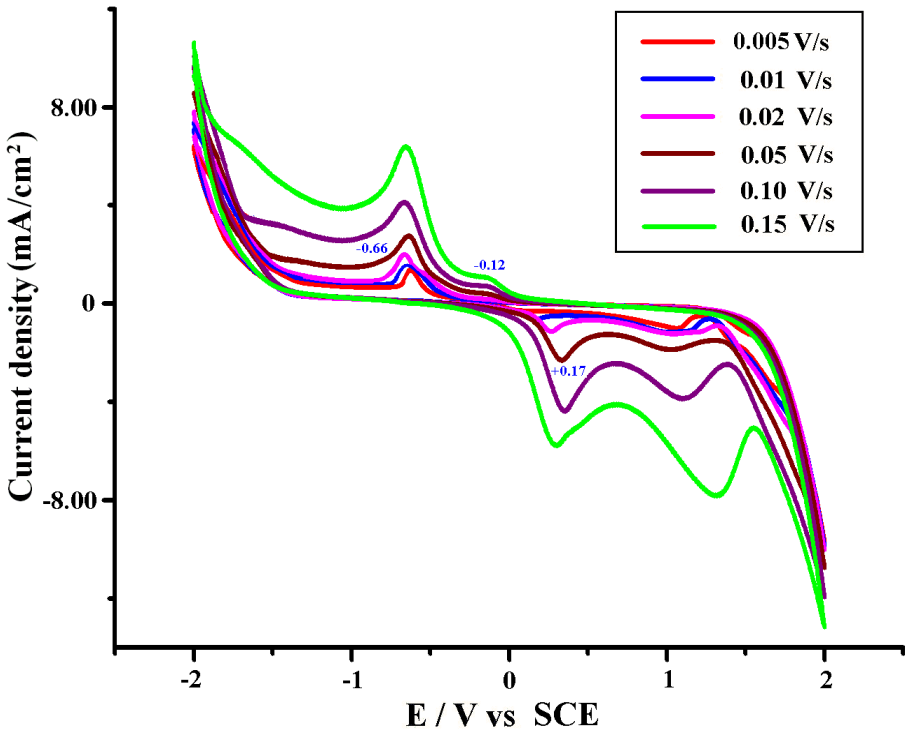

Fig. S12 CVs of **1-GCE** in 0.05 M phosphate buffer aqueous solution (pH = 6.8, H_3PO_4/KOH, 50 mL) at 50 ℃ at different sweep rates.

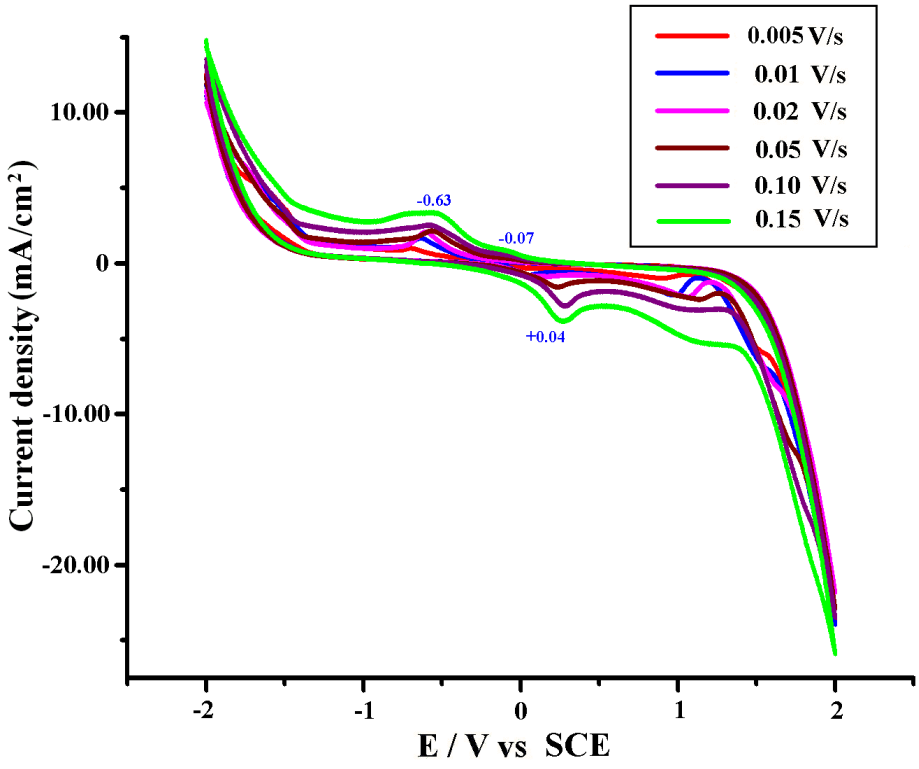

Fig. S13 CVs of **1-GCE** in 0.05 M phosphate buffer aqueous solution (pH = 6.8, H_3PO_4/KOH, 50 mL) at 80 ℃ at different sweep rates.

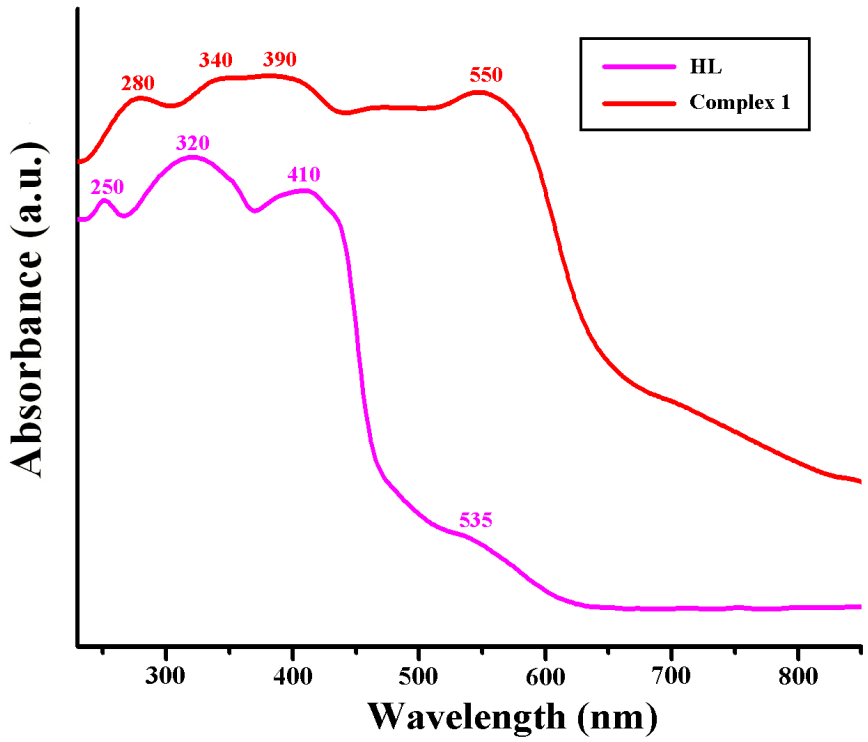

Fig. S14 UV-vis absorption spectra at room temperature for the free organic ligand **HL** and complex **1**.

The Electrochemical Property of Nanosized Pt In order to evaluate the electrocatalytic property of complex **1** for the HER from water, the electrochemical property of nanosized Pt was measured in comparison. Herein, the nanosized Pt was commercially purchased from Beijing HWRK chemical Co., LTD. The powder XRD of the sample was shown in **Fig. S15**, which matches well with the standard cubic Pt with lattice constants a = b = c = 3.924 Å (JCPDS 65-2868). The SEM images of the nanosized Pt were shown in **Fig. S16**. Similarly, 4 mg Pt powder was modified on the **GCE**, as shown in **Fig. S17**.

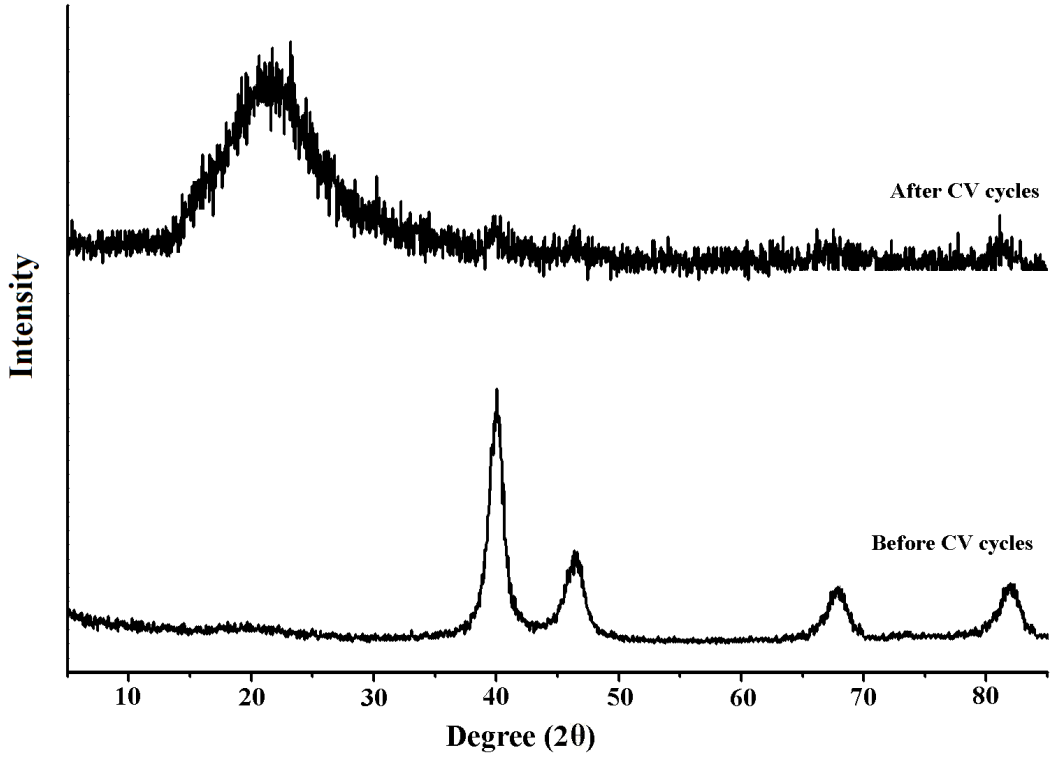

Fig. S15 The powder XRD patterns for the Pt powder.

(a)

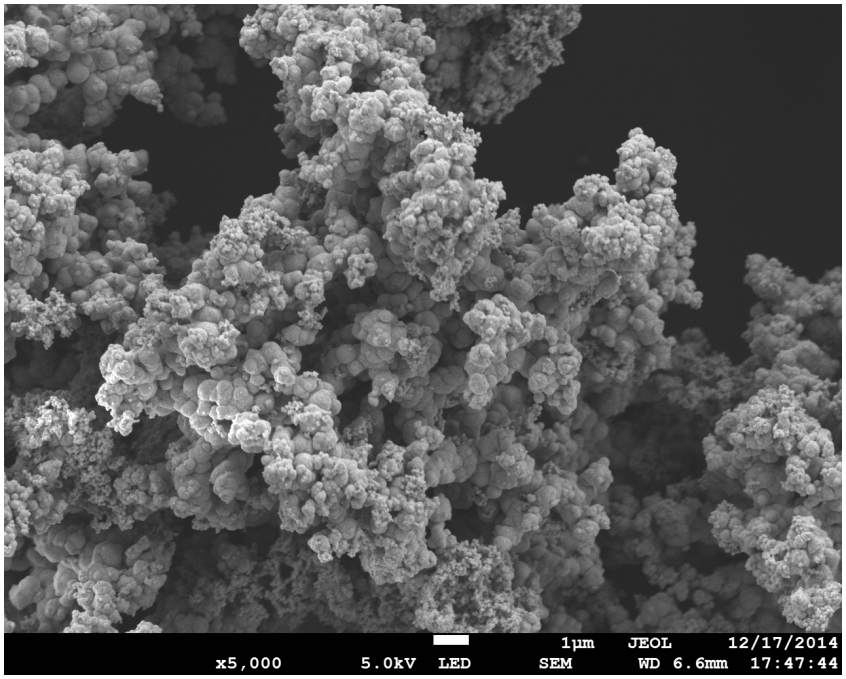

(b)

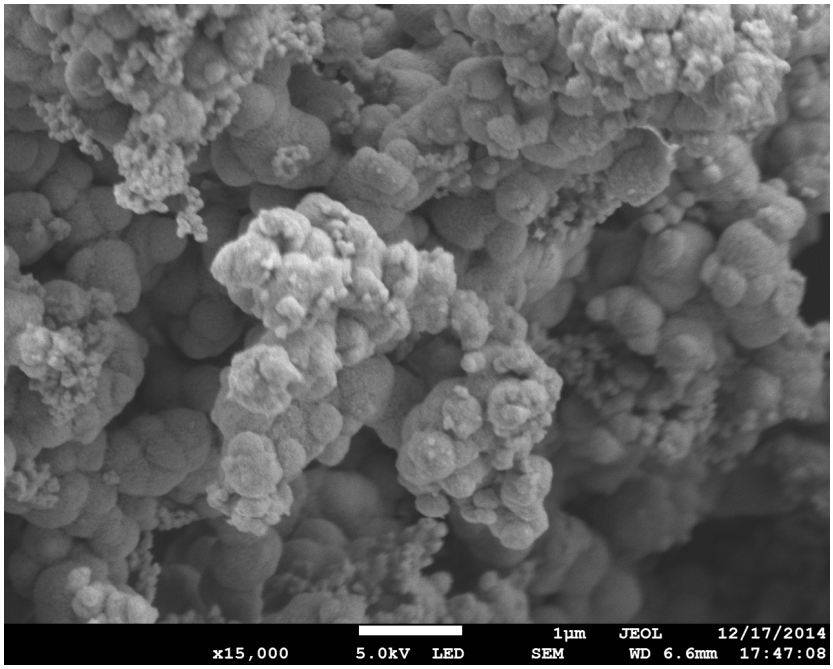

Fig. S16 The SEM images of the nanosized Pt.

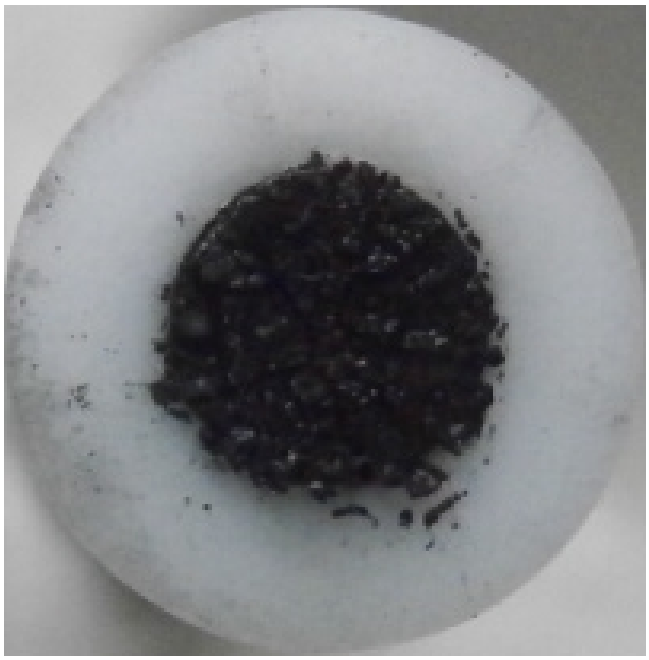

Fig. S17 The image of the **Pt-GCE**.

The CVs were also measured at 30 ℃ in 0.05 M phosphate buffer aqueous solution (pH = 6.8, H_3PO_4/KOH, 50 mL) in a three-electrode cell with a SCE and a platinum foil used as the reference and counter electrode, respectively. The first CV cycle at the **Pt-GCE** are shown in **Fig. S18** and **Fig. S19**. Much higher HER current and lower overpotential are observed at the nanosized **Pt-GCE** with respect to the bare **GCE** and **1-GCE**, indicating the nanosized Pt possesses much better electrocatalytic activity than complex **1**, which is in agreement with our expectation.

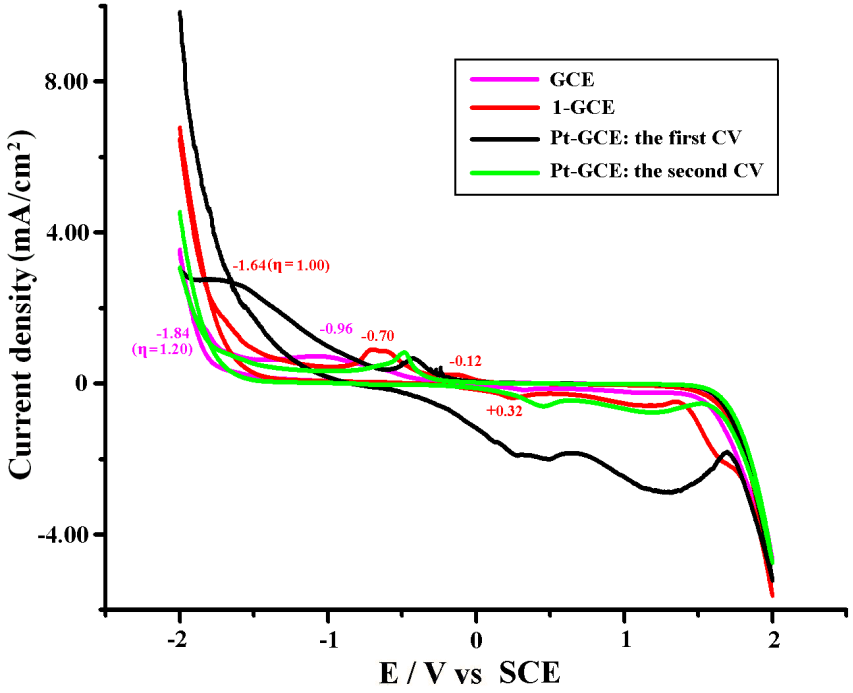

Fig. S18 CVs of the bare **GCE**, **1-GCE** and **Pt-GCE** in 0.05M phosphate buffer aqueous solution (pH = 6.8, H_3PO_4/KOH, 50 mL) at a sweep rate of 0.01 $V \cdot s^{-1}$ at 30 ℃. The black and green curves indicate the first and second CV cycle at the Pt-GCE, respectively.

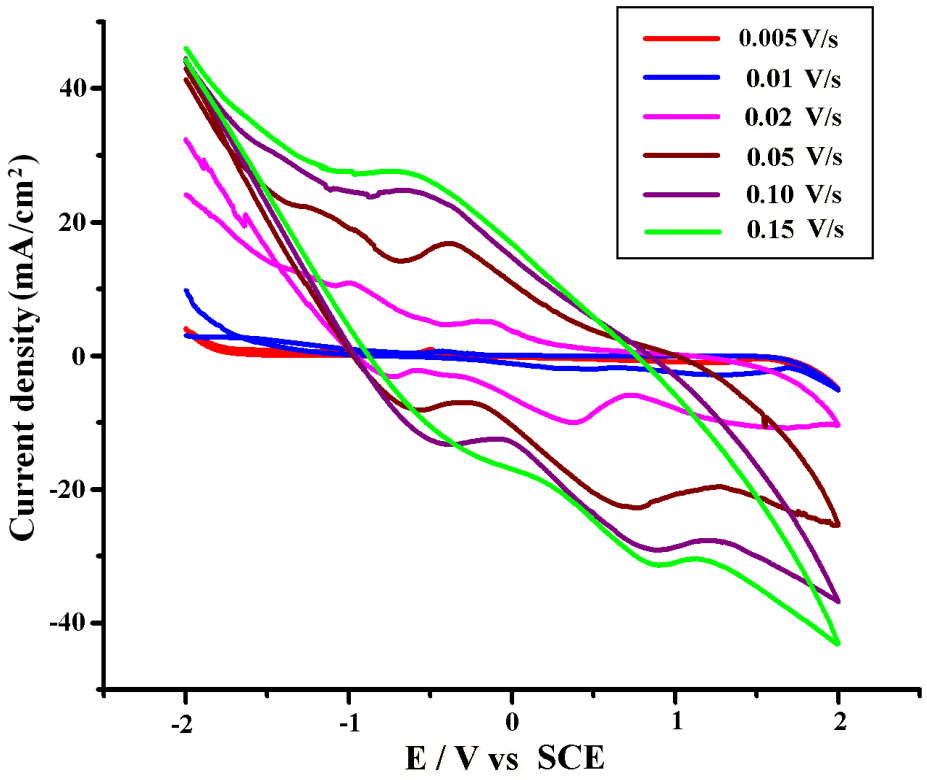

Fig. S19 The first CV cycle at the **Pt-GCE** in 0.05 M phosphate buffer aqueous solution (pH = 6.8, H_3PO_4/KOH, 50 mL) at 30 ℃ at different sweep rates.

However, the second CV cycle at the **Pt-GCE** is quite different from the first CV cycle, as shown in **Fig. S18** and **Fig. S20.** Under the room temperature of 30 °C, the second CV cycle reveals the potential for the HER at the **Pt-GCE** was more negative to **1-GCE**, indicating the nanosized Pt shows worse electrocatalytic activity for the HER than complex **1** in the second CV cycle. It is expected that the nanosized Pt is too active to lose its activity, and the nano-Pt is probably to be poisoned in the second CV cycle. And the powder XRD of the solid sample left on the **Pt-GCE** after the electrochemical experiment shows the sample is amorphous, as shown in **Fig. S15**. The detailed reason is under investigation.

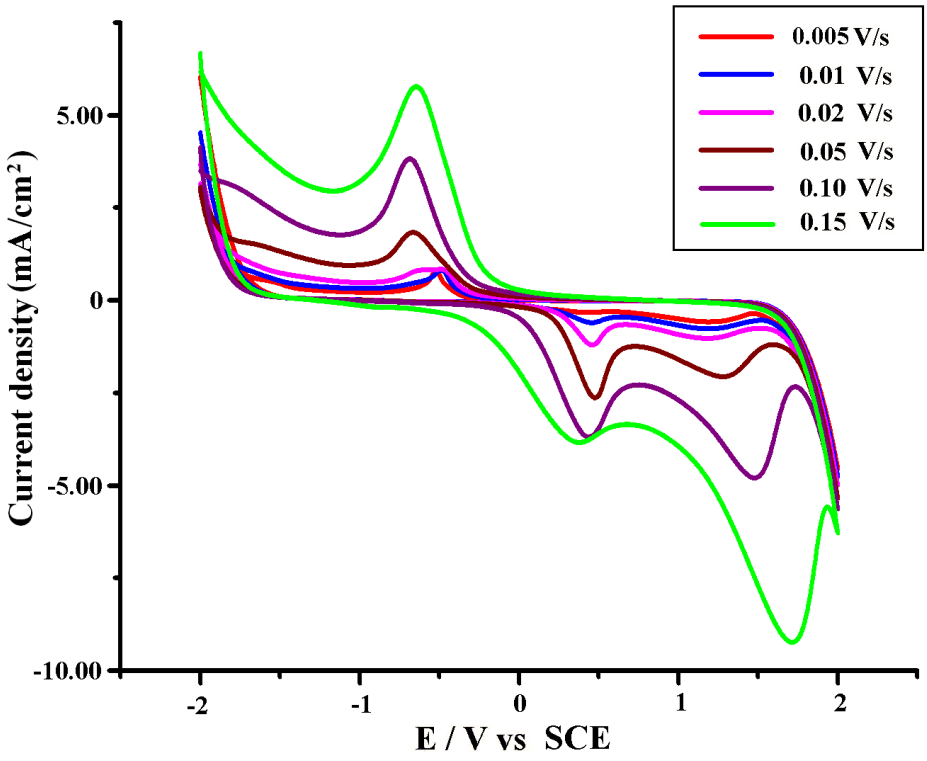

Fig. S20 The second CV cycle at **Pt-GCE** in 0.05 M phosphate buffer aqueous solution (pH = 6.8, H_3PO_4/KOH, 50 mL) at 30 ℃ at different sweep rates.

References:

1 Y. J. Sun, J. P. Bigi, N. A. Piro, M. L. Tang, J. R. Long and C. J. Chang, *J. Am. Chem. Soc.*, **2011**, *133*, 9212.